Long-range intermolecular charge transfer induced by laser pulses: an explicitly time-dependent configuration interaction approach

Stefan Klinkusch, Tillmann Klamroth* and Peter Saalfrank

Received 13th October 2008, Accepted 20th February 2009
First published as an Advance Article on the web 13th March 2009
DOI: 10.1039/b817873a

In this paper, we report simulations of laser-driven many-electron dynamics by means of the time-dependent configuration interaction singles (TD-CIS) approach. The method is capable of describing explicitly time-dependent phenomena beyond perturbation theory and is systematically improvable. In contrast to most time-dependent density functional methods it also allows us to treat long-range charge-transfer states properly. As an example, the laser-pulse induced charge transfer between a donor (ethylene) and an acceptor molecule (tetracyanoethylene, TCNE) is studied by means of TD-CIS. Also, larger aggregates consisting of several donors and/or acceptors are considered. It is shown that the charge distribution and hence the dipole moments of the systems under study are switchable by (a series of) laser pulses which induce selective, state-to-state electronic transitions.

1. Introduction

Electron transfer processes are ubiquitous and of general importance in chemistry. Examples are the formation of charge-transfer complexes, the photophysics of metal complexes, redox reactions, electrochemistry, STM-induced processes and biological function. Often, the charge transfer (CT) is long-range and induced *via* optical excitation. In the present work, intermolecular charge transfer driven by ultrashort laser pulses will be considered.

After the pioneering work of Zewail and coworkers in the field of "femtochemistry",[1,2] the timescale for detection and control, of ultrafast molecular processes has meanwhile been pushed into the attosecond domain.[3,4] On such short timescales the electron motion can be observed and controlled, while the motion of nuclei still plays no role. It is the goal of the present paper to model the long-range, intermolecular charge transfer by ultrashort laser pulses.

For this purpose a many-electron method is required which is explicitly time-dependent and which goes beyond perturbation theory to make the action of intense laser pulses tractable. Time-dependent density functional theory (TD-DFT) is one such approach.[5] While formulated in most applications in the linear response regime,[6,7] explicitly time-dependent variants are also known and in use. Despite being efficient, most versions of TD-DFT have the disadvantage of not being able to properly account for long-range charge transfer.[7–13] For example, the excitation energy for a charge transfer from a molecular donor (D) to an acceptor (A) is given asymptotically, *i.e.* for $R \rightarrow \infty$, as (atomic units)

$$\omega_{\mathrm{CT}}(R) = \mathrm{IP(D)} - E_{\mathrm{A}}(\mathrm{A}) - \frac{1}{R}. \qquad (1)$$

Institut für Chemie, Universität Potsdam, Karl-Liebknecht-Str. 24-25, D-14476 Potsdam-Golm, Germany. E-mail: klamroth@uni-potsdam.de

Here, IP(D) is the ionization potential of the donor, EA(A) the acceptor's electron affinity and R is the distance between D and A. In deviation from eqn (1), TD-DFT with pure density functionals gives ω_{CT} as the difference between the Kohn–Sham orbital energies of the LUMO of the acceptor and the HOMO of the donor. As a consequence, there is almost no R-dependence of ω_{CT} in this case. It is known that this failure is due to the absence of "exact", Hartree–Fock-like exchange.[7] When using hybrid functionals such as B3LYP[14] with a certain fraction x (<1) of exact exchange ($x = 0.20$ for B3LYP), the asymptotic behaviour of a charge transfer state is partially corrected to $-\frac{x}{R}$.

In contrast, the time-dependent configuration interaction (TD-CI) method[15–18] is free from such problems, because exchange is "exact". Further, the method can be systematically improved towards the full-CI limit by taking successively higher excitations into account: single excitations (TD-CIS), single and double excitations, exact or perturbative (TD-CISD and TD-CIS(D)), triple excitations (TD-CISDT) and so forth. So far, the method was applied in one-dimensional model problems, for laser-induced transport[15] and photoionization.[16] For real three-dimensional molecular systems, TD-CI was used for laser-driven state-to-state transitions (including intramolecular charge transfer),[19–21] the creation of electronic wavepackets, and for the calculation of (non-linear) molecular response following short-pulse excitation.[18,22] In passing we note that the method has also been extended to dissipative systems.[23] Furthermore, the TD-CI method can be viewed as a special variant of the more general explicitly time-dependent CASSCF (complete active space self-consistent field) method, also called MCTDHF (multi-configurational time-dependent Hartree–Fock), in which both the configurations and their coefficients are explicitly time-dependent.[24–26] Here, the performance of the TD-CIS method for long-range, intermolecular charge transfer processes will be tested.

The paper is organized as follows. In section 2 we sketch the TD-CIS approach as well as the molecule-field coupling, which is treated in the semiclassical dipole approximation. In section 3 we apply the method to laser-induced charge transfer in a model donor–acceptor system, with D = ethylene and A = tetracyanoethylene (TCNE) arranged in a stacked geometry. Also larger systems, consisting of several donors and/or acceptors, will be studied. Section 4 summarizes the paper.

Unless otherwise stated all quantities in this work will be given in atomic units, *i.e.* energies will be measured in E_h (Hartree), lengths in a_0 (Bohr), time in atomic time units $\hbar/E_h$, dipole moments in units of ea_0 (where e is the elementary charge), and field strengths as multiples of E_h/ea_0. If no units are explicitly indicated, atomic units are meant.

2. Theoretical methods

2.1 The TD-CIS method

Our goal is to solve the time-dependent electronic Schrödinger equation

$$i\frac{\partial\Psi(t)}{\partial t} = [\hat{H}_0 - \hat{\vec{\mu}}\vec{F}(t)]\Psi(t). \tag{2}$$

Here, $\hat{H}_0$ is the field-free electronic Hamiltonian of a molecule consisting of N electrons in the field of N_A fixed nuclei,

$$\hat{H}_0 = -\frac{1}{2}\sum_{i=1}^{N}\Delta_i + \sum_{i=1}^{N}\sum_{j>i}^{N}\frac{1}{r_{ij}} - \sum_{A=1}^{N_A}\sum_{i=1}^{N}\frac{Z_A}{r_{Ai}} \tag{3}$$

where $r_{ij} = |\vec{r}_i - \vec{r}_j|$ and $r_{Ai} = |\vec{R}_A - \vec{r}_i|$ denote interelectronic and electron-nuclei distances, respectively. Z_A is the nuclear charge of atom A, $\hat{\vec{\mu}} = -\sum_{i=1}^{N}\vec{r}_i + \sum_{A=1}^{N_A}Z_A\vec{R}_A$ the dipole operator, and $\vec{F}(t)$ the laser field, which is assumed to be coordinate-independent under the dipole approximation.

In the TD-CIS method, the electronic wave function is expanded as

$$\Psi(t) = \sum_i C_i(t)\Psi_i^{\mathrm{CIS}} \tag{4}$$

with the coefficients $C_i(t) = \langle\Psi(t)|\Psi_i^{\mathrm{CIS}}\rangle$ being in general explicitly time-dependent. The CIS state functions are time-independent. When restricting to optical transitions between singlet states only, they are given as

$$\Psi_i^{\mathrm{CIS}} = D_{0,i}\Psi_0^{\mathrm{HF}} + \sum_a\sum_r D_{a,i}^r\,{}^1\Psi_a^r. \tag{5}$$

Here, Ψ_0^{HF} is the Hartree–Fock (HF) ground-state Slater determinant. ${}^1\Psi_a^r = \frac{1}{\sqrt{2}}(\Psi_a^r + \Psi_{\bar{a}}^{\bar{r}})$ are singlet configuration state functions. These arise from single excitations of an α electron from spatial orbital a to the virtual orbital r, Ψ_a^r, and the corresponding excitation of a β orbital ($\Psi_{\bar{a}}^{\bar{r}}$). The inner coefficient vectors $\vec{D}_i = (D_{0,i}; \{D_{a,i}^r\})$ can be calculated from the secular equation

$$\mathbf{H}^{\mathrm{CIS}}\vec{D}_i = E_i^{\mathrm{CIS}}\vec{D}_i. \tag{6}$$

In eqn (6), E_i^{CIS} is the energy for the state i and $\mathbf{H}^{\mathrm{CIS}}$ is a Hamiltonian matrix with the elements $H_{IJ}^{\mathrm{CIS}} = \langle\Psi_I|\hat{H}_0|\Psi_J\rangle$, where Ψ_I and Ψ_J are HF or singly excited configuration state functions, all of them singlets. Of course, the CIS ground state is the HF Slater determinant, with energy $E_0^{\mathrm{CIS}} = E_0^{\mathrm{HF}}$.

For the propagation of the outer coefficients $\vec{C}(t) = (C_0, C_1, \ldots)$, an operator splitting technique is used:[27]

$$\vec{C}(t+\Delta t) = \left[\prod_{q=x,y,z}\mathbf{U}_q^{\dagger}e^{iF_q(t)\boldsymbol{\mu}_q\Delta t}\mathbf{U}_q\right]e^{-i\tilde{\mathbf{H}}\Delta t}\vec{C}(t). \tag{7}$$

In eqn (7), $\tilde{\mathbf{H}}$ is a diagonal Hamiltonian matrix in the CI eigenstate basis. $\mathbf{U}_q$ is a unitary matrix which transforms the wave function from the CI eigenstate basis to a basis where the dipole matrix $\boldsymbol{\mu}_q$ is diagonal and $F_q(t)$ is the electric laser field, linearly polarized along the coordinate q. Eqn (7) is used when the laser is on. As soon as the laser is switched off, at a time t_f, say, the time-dependence of the wave function is trivially through phase factors only, and analytically given as

$$\Psi(t_f + \Delta t) = \sum_i C_i(t_f)e^{-iE_i^{\mathrm{CIS}}\Delta t}\Psi_i^{\mathrm{CIS}}. \tag{8}$$

2.2 Laser pulses

In this work, two different classes of laser pulses are simulated. For one part, we adopt simple π-pulses or sequences of π-pulses. π-Pulses are known to lead to a population inversion in an idealized two-level system and under the rotating wave approximation (RWA).[28] The field is of $\cos^2$ shape

$$\vec{F}(t) = \vec{f}(t)\cos[\omega(t - t_p)], \tag{9}$$

$$\vec{f}(t) = \begin{cases}\vec{f}_0\cos^2\left[\frac{\pi}{2\sigma}(t-t_p)\right] & \text{if } |t-t_p| < \sigma \\ 0 & \text{else}\end{cases}. \tag{10}$$

Here, t_p is the time when the pulse is maximal, σ its full width at half maximum, ω the laser frequency, and $\vec{f}_0$ is the value of the shape function at $t = t_p$. Let further $\vec{\mu}_{fi}$ be the transition dipole moment for the transition from an initial state $|i\rangle$ to a final state $|f\rangle$. Then, if $\vec{f}_0$ and $\vec{\mu}_{fi}$ are parallel to each other, the π-pulse condition is

$$|\vec{f}_0| = \frac{\pi}{\sigma|\vec{\mu}_{fi}|} \tag{11}$$

The second class of laser pulses employed in the simulation here are constructed from optimal control theory (OCT).[29,30] Here, an algorithm of Rabitz *et al.*[31–33] is used. Accordingly, we maximize the expectation value of a positive target operator $\hat{O}$ at the end of the control time, t_f, under the two additional conditions that the laser field intensity should be as low as possible and the time-dependent Schrödinger equation must be fulfilled. Thus, the functional

$$\begin{aligned} J = &\langle\Psi(t_f)|\hat{O}|\Psi(t_f)\rangle - \int_0^{t_f}\alpha(t)|\vec{F}(t)|^2\,\mathrm{d}t \\ &- 2\mathrm{Re}\left[\int_0^{t_f}\langle\chi(t)|\frac{\partial}{\partial t} + i(\hat{H}_0 - \hat{\vec{\mu}}\vec{F}(t))|\Psi(t)\rangle\,\mathrm{d}t\right] \end{aligned} \tag{12}$$

is to be maximized. In this equation, $\chi(t)$ is a Lagrange multiplier and $\alpha(t)$ a user-specified, positive constraint function. The latter is chosen here as

$$\alpha(t) = \frac{\alpha}{g(t)}, \tag{13}$$

where α is a penalty factor and $g(t)$ an exponential

$$g(t) = \mathrm{e}^{-\left(\frac{t-t_\mathrm{m}}{\Delta t_\mathrm{s}}\right)^{N_\mathrm{s}}} \tag{14}$$

with parameters t_m (time in the middle of the shape function, m = middle), Δt_s (width of the shape function, s = shape function) and N_s (exponent of the Gaussian shape function). Their values will be given later.

From the condition $\delta J = 0$, the laser field is obtained from three equations, which can be solved iteratively. The first one is the Schrödinger equation (2), the other two are

$$\mathrm{i}\frac{\partial\chi(t)}{\partial t} = [\hat{H}_0 - \hat{\vec{\mu}}\vec{F}(t)]\chi(t) \text{ with } \chi(t_\mathrm{f}) = \hat{O}\Psi(t_\mathrm{f}) \tag{15}$$

and

$$\vec{F}(t) = -\frac{1}{\alpha(t)}\mathrm{Im}[\langle\chi(t)|\hat{\vec{\mu}}|\Psi(t)\rangle]. \tag{16}$$

Eqn (2) is solved by forward propagation with the initial condition $\psi(t_0) = \Psi_0^{\mathrm{HF}}$, eqn (15) is solved by backward propagation with the initial condition $\chi(t_\mathrm{f}) = \hat{O}\Psi(t_\mathrm{f})$. The target operator is typically a projector onto one of the CIS states, $\hat{O} = |\Psi_i^{\mathrm{CIS}}\rangle\langle\Psi_i^{\mathrm{CIS}}|$. The field is calculated from eqn (16) in each iteration. The procedure is repeated until convergence is achieved.

3. Results and discussion

3.1 A donor–acceptor system: DA

3.1.1 Stationary quantum chemistry. For our model donor–acceptor system ethylene as a donor and tetracyanoethylene as the acceptor were chosen. First, a geometry optimization on the RHF (restricted Hartree–Fock)/6-31G*[34] level of theory was carried out with the GAUSSIAN 03[35] program package. As a result, both molecules are almost flat and stacked above each other as shown in Fig. 1 in the equilibrium geometry. There are only slight changes of internal geometry parameters, relative to the free molecules.

By using the optimized geometries for the two molecules ethylene and TCNE and only varying the donor–acceptor distance while keeping all (internal) geometry parameters intact, the ground state (S_0) potential energy curve shown as the lowest curve in Fig. 2 (left) was obtained. We note that this curve predicts a shallow minimum at $R_0 = 7.2\ a_0$, close to the fully optimized structure shown in Fig. 1. Of course, the ground-state potential is unreliable on the HF level of theory, because van der Waals and π–π interactions are not accounted for in this uncorrelated method. (Not even basis-set superposition errors have been corrected.) Of course, the precise geometry and wavefunctions can be important for quantitative predictions; here, however, we focus on the long-range charge transfer process and effects due to van-der-Waals-type interactions are not considered. A similar

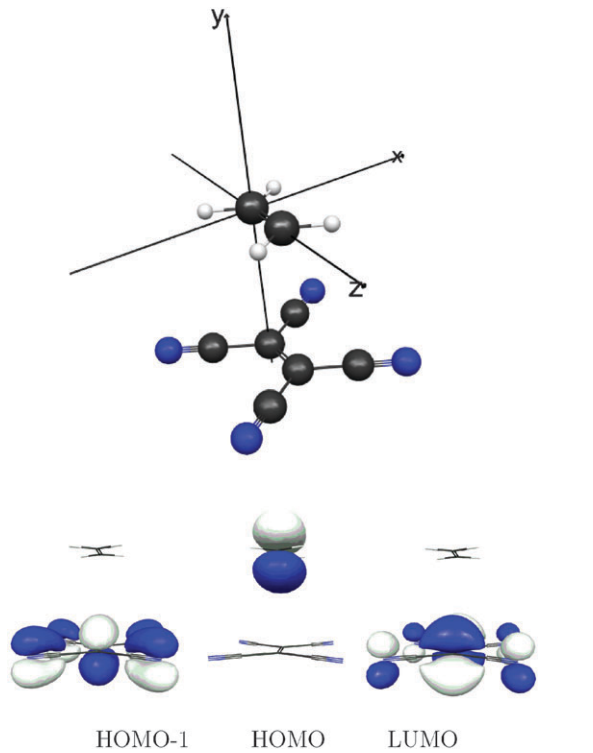

Fig. 1 The upper panel shows the ethylene–tetracyanoethene system at its RHF/6-31G* equilibrium geometry, together with the definition of the coordinate system employed in this work. The lower panel is a pictorial representation of the HOMO-1 (equivalent to HOMO(A) = π(A)), the HOMO (equivalent to HOMO(D) = π(D)), and the LUMO (equivalent to LUMO(A) = π*(A)) of the complex.

ground state potential curve is obtained with density functional theory. Using the (pure) exchange–correlation functional BP86 according to Becke and Perdew[36,37] and 6-31G*, the lowest curve on the right panel of Fig. 2 is obtained. Its absolute energy is about 3 E_h lower than the HF S_0 curve, because of correlation. Also, the minimum at the ground-state curve is somewhat deeper than for HF (= CIS), at around the same equilibrium distance.

Excited-state potential energy curves were then computed on the CIS/6-31G* and (linear-response) TD-BP86/6-31G* levels of theory. Using CIS, altogether 4145 singlet states were obtained which will all be used in the dynamics calculations below. For this purpose, one- and two-electron integrals of the atomic orbital basis were taken from a GAMESS[38] RHF calculation; the rest of the program was written from scratch.

As expected, there is a bound charge-transfer state in the CIS picture as shown in Fig. 2, left. This can be seen from the fact that several excited potential energy curves are bending upwards and are close to the model, lowest charge-transfer curve

$$V_\mathrm{CT} = V_{\mathrm{S}_0}(R) + \omega_\mathrm{CT}(R), \tag{17}$$

with $\omega_\mathrm{CT}(R)$ defined in eqn (1). Two model charge-transfer curves are shown as black, dashed curves in Fig. 2, referring to different methods to calculate the ionization potential and the electron affinity in eqn (1). The thin-dashed curve refers to Koopmans' theorem (*i.e.* IP(D) = $-\varepsilon_\mathrm{HOMO}$(D),

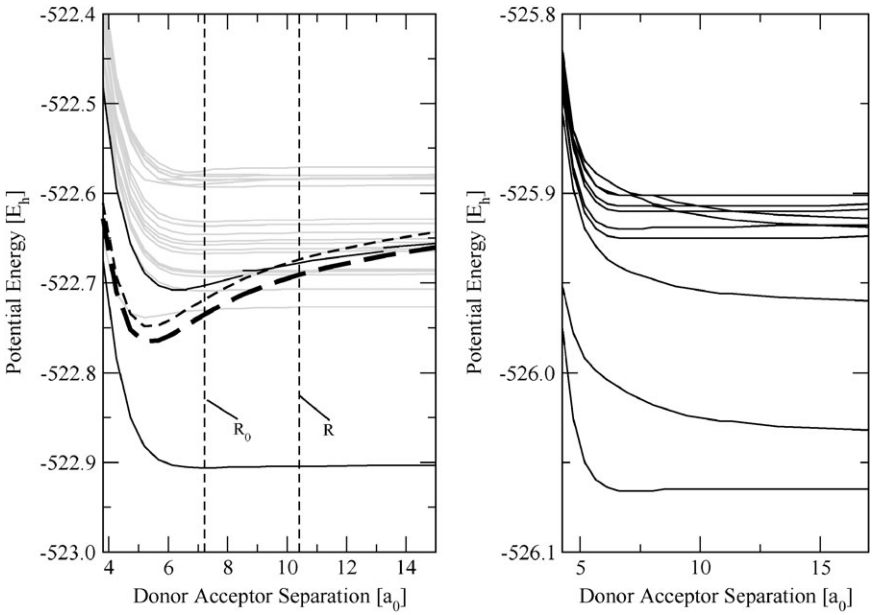

Fig. 2 Potentials of the electronic ground state and several excited states, calculated with CIS/6-31G* (left) and with TD-BP86/6-31G* (right). On the left panel, two ideal charge-transfer potentials according to eqn (17) are shown as dashed lines. For the thin dashed line, $\omega_{CT}(R)$ [defined in eqn (1)] has been calculated according to Koopmans' theorem, while the long-dashed curve represent is obtained from a CIS calculation at a long distance, see text. Black, solid potential energy curves and segments of adiabatic excited state curves represent the electronic ground state and the excited CT state, respectively. Other potential curves are drawn in grey for clarity.

EA(A) = $-\varepsilon_{LUMO}$(A), with ε denoting Hartree–Fock orbital energies), while the long-dashed curve represents the result of a CIS calculation at a long distance, $R = 35\ a_0$. Both are, of course, parallel to each other and have the correct $1/R$ behaviour, with the latter, however, being more realistic. At around the equilibrium distance R_0 of the ground state, indicated by a vertical line in the Figure, the second excited state S_2 is close to the ideal charge transfer state, while at larger distances R higher CIS states correspond to the charge-transfer state. For instance, at $R = 10.4\ a_0$ (the second vertical line in the Figure), state S_6 is the transfer state. At $R_0 = 7.2$, the CIS excitation energy to the charge transfer state S_2 is about 0.192, at $R = 10.4$ the excitation energy to S_6 is roughly 0.235. The ideal values ω_{CT}, calculated from Koopmans' ionization potentials and electron affinities of the free molecules, IP(D) = 0.37420 and EA(A) = 0.04796, give $\omega_{CT} = 0.187$ at R_0 and $\omega_{CT} = 0.230$ at $R = 10.4$, respectively. If the model values are calculated from the CIS states, they give $\omega_{CT} = 0.170$ at R_0 and $\omega_{CT} = 0.213$ at $R = 10.4$. Note that the excited CIS states are adiabatic. This is different for the model charge-transfer curve (17), which is why the character of individual CIS states changes along R, and avoided crossings become visible. The change of character of the adiabatic CIS curves and the avoided crossings along R are indicated by showing the CT curve (segments) in black, and all others in grey.

Analysis of the CIS CT state shows, that it is dominated by a HOMO(D) → LUMO(A) transition. HOMO(D) is the π-orbital of ethylene, and LUMO(A) the π*-orbital of TCNE. These orbitals are also the HOMO and LUMO of the ethylene–TCNE complex, both shown in Fig. 1. The $S_0 \rightarrow S_1$ excitation, on the other hand, is an almost ideal π → π* transition within the acceptor molecule, corresponding to a HOMO-1 → LUMO transition within the complex (see Fig. 1).

In contrast to CIS, for TD-BP86 there is no bound charge-transfer state. Some of the excited states are even strongly repulsive as can be seen from Fig. 2, right panel: TD-BP86 fails to produce a reliable CT state for the reasons given above.

In Table 1, the energies and (transition) dipole moments of the lowest three CIS states for the fully optimized ethylene–TCNE complex as shown in Fig. 1 (upper panel) are given. The coordinate system was chosen as indicated in that Figure, with the molecular axes denoted as the z-direction and the perpendicular coordinate being y.

From the Table we first of all note that the energies are slightly different from those anticipated from Fig. 2, which is due to the fact that now we refer to the fully optimized structure. We observe a big change in the dipole moment when going from the electronic ground state to the second excited state. Ideally, this corresponds to a transfer of an electron from ethylene to TCNE, resulting in an ideal change of the dipole moment of $eR_0 = 7.2\ ea_0$. In practice, a value around 6 ea_0 is observed. The charge transfer is not quite complete at this distance, as supported by the Mulliken populations which suggest a charge of +0.003 e

Table 1 Energies E_n, excitation energies E_n^{exc}, dipole moments along y, $\mu_{nn,y}$ and selected transition dipole moments $\mu_{n0,z}$ and $\mu_{n1,y}$ for certain states S_n in the donor–acceptor system. All values were calculated with CIS/6-31G* at the equilibrium geometry, and are given in atomic units

S_n	E_n	E_n^{exc}	$\mu_{nn,y}$	$\mu_{n0,z}$	$\mu_{n1,y}$
0	−522.9529	0.0000	0.0822	—	−0.0036
1	−522.7489	0.2040	1.0374	1.8120	—
2	−522.7322	0.2207	6.0883	−0.8583	2.3963

Table 2 The character table for the point group C_{2v}, adapted for the coordinate system used here

C_{2v}	E	C_2	$\sigma_v(yz)$	$\sigma'_v(xy)$	
A_1	1	1	1	1	y
A_2	1	1	−1	−1	—
B_1	1	−1	1	−1	z
B_2	1	−1	−1	1	x

and −0.003 e for ethylene and TCNE in S_0, and +0.842 e and −0.842 in S_2.

Most of the components of the transition dipole moment not shown in the table, for example $\mu_{20,x}$, $\mu_{20,y}$, $\mu_{21,x}$, or $\mu_{21,y}$, are exactly or almost exactly zero by symmetry: the $S_0 \rightarrow S_1$ and $S_0 \rightarrow S_2$ transitions are z-polarized, while $S_1 \rightarrow S_2$ is y-polarized. These selection rules are easily understood from the point group symmetry of the DA complex, which is (almost exactly) C_{2v}. Using the coordinate system shown in Fig. 1, the C_{2v} character table is given as in Table 2.

The three transitions of interest, $S_0 \rightarrow S_1$, $S_1 \rightarrow S_2$, and $S_0 \rightarrow S_2$, are, in a simple orbital picture, $\pi(A) \rightarrow \pi^*(A)$, $\pi(D) \rightarrow \pi(A)$, and $\pi(D) \rightarrow \pi^*(A)$, respectively. Since every π-orbital transforms as A_1, a $\pi \rightarrow \pi$-transition must be y-polarized to ensure $A_1 \otimes A_1 \otimes A_1 = A_1$. In contrast, every π*-orbital is B_1, such that z-polarized pulses (with $z \sim B_1$) are needed for $\pi \rightarrow \pi^*$-transitions: $A_1 \otimes B_1 \otimes B_1 = A_1$.

3.1.2 Laser-induced charge-transfer dynamics. According to these symmetry rules, there are different ways to excite the CT state S_2 from the ground state S_0 at the equilibrium geometry. First, there is the *direct* π-pulse excitation from S_0 to S_2, using a z-polarized laser. Secondly, we can use an *indirect* route with a sequential excitation $S_0 \rightarrow S_1$ and then $S_1 \rightarrow S_2$ with two π-pulses, the first one z-, the second one y-polarized. In the direct pathway, an electron is directly transferred from D to A, while in the indirect process a "hole" is first created in A, which then hops to D (see below). Third, there is the possibility to use optimal control theory which selects its own, optimal pathway.

Direct excitation $S_0 \rightarrow S_2$. First, the direct $S_0 \rightarrow S_2$ transition with z-polarized π-pulses and different pulse lengths was attempted. The time-evolution of the dipole moment perpendicular to the molecular planes is shown in Fig. 3, with the direct charge-transfer mechanism sketched in the upper panel. We note that for "long" pulses, *e.g.* $\sigma = 2000$ atomic time units (or about 48 fs), an almost complete switching of the initial to the target state is possible, with a final-state population $P(S_2;t_f) = 0.999$. (Here, $t_f = 2\sigma$ is when the total pulse ends.) This corresponds to a dipole change from 0.08, to about 6.09 according to Table 1.

When shorter pulses are used, $\sigma = 1000$ (or about 24 fs), the target state population is about 0.994. In this case also small oscillations of the dipole moment become visible, indicative of the creation of an electronic wavepacket. The oscillation period τ of about 370 atomic time units corresponds to an energy difference $\omega = 2\pi/\tau$ of about 0.0168 E_h, which nicely fits to the energy difference between S_1 and S_2, of 0.0167. In general, the dipole moment oscillates as $\mu_y(t) = \sum_i \sum_j C_i(t_f) C_j(t_f) e^{i\omega_{ij}t} \langle \Psi_i^{CIS} | \hat{\mu}_y | \Psi_j^{CIS} \rangle$

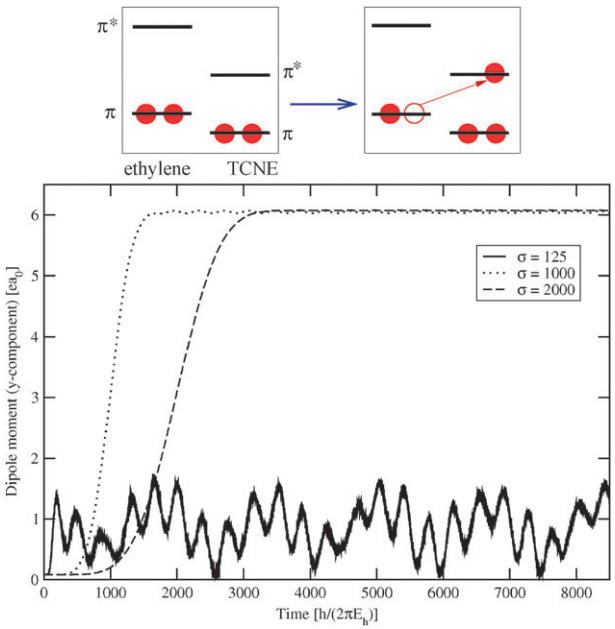

Fig. 3 Upper panel: schematic representation of the "direct" scheme. Lower panel: the dipole moment (y-component) for the DA system for various π-pulses are applied. The time step of the propagation is $\Delta t = 0.10$. The pulse parameters are, for $\sigma = 125$: $t_p = \sigma = 125$, $f_{0,z} = 0.0293$, $\omega = 0.2207$. For $\sigma = 1000$: $t_p = 1000$, $f_{0,z} = 0.0037$, $\omega = 0.2207$. For $\sigma = 2000$: $t_p = 2000$, $f_{0,z} = 0.0018$, $\omega = 0.2207$.

where $\omega_{ij} = E_i^{CIS} - E_j^{CIS}$, showing that the transition dipole moments determine the amplitude of the oscillations.

With even shorter pulses, due to the higher intensities multi-photon excitations come into play. For a very short pulse, $\sigma = 125$ (about 3 fs), for example, a wave packet containing at least three different oscillation periods is formed. Thus, also higher states are significantly populated, at the expense of S_2, which carries a target state population of only 0.180 at the end of the pulse. Since very high states can be reached, converged TD-CIS calculations for very short pulses typically require the use of all singly excited states.

For completeness we note that the maximal intensities of the three π-pulses are 1.1×10^{11} W cm^{-2} ($\sigma = 2000$), 4.8×10^{11} W cm^{-2} ($\sigma = 1000$), and 3.0×10^{13} W cm^{-2} ($\sigma = 125$) respectively. The corresponding laser pulse fluences are 4.1 mJ cm^{-2} ($\sigma = 2000$), 8.7 mJ cm^{-2} ($\sigma = 1000$), and 68.3 mJ cm^{-2} ($\sigma = 125$).

Optimal control theory. The bad performance of ultrashort π-pulses raises the question as to whether optimal control theory would do better. For this purpose a random pulse with carrier frequency ω_{20} and total pulse length $t_f = 2\sigma = 250$ was used as the initial field for the OCT algorithm, and iteratively improved. The further control parameters of eqn (13) and (14) were chosen as $\alpha = 3.2 \times 10^{-13}$ [$(E_h/ea_0)^2$], $t_m = 125$, $\Delta t_s = 220$, and $N_s = 12$. After 20 OCT iterations, a target state population of about 0.420 is obtained *versus* 0.180 for the original π-pulse as seen from the middle panel of Fig. 4. The intensity of the electric field of the OCT pulse is even lower than that of the π-pulse, which suppresses multi-photon excitations. Still, the pulse laser frequency is close to the π-pulse one, indicative of a dominantly direct $S_0 \rightarrow S_2$ transition

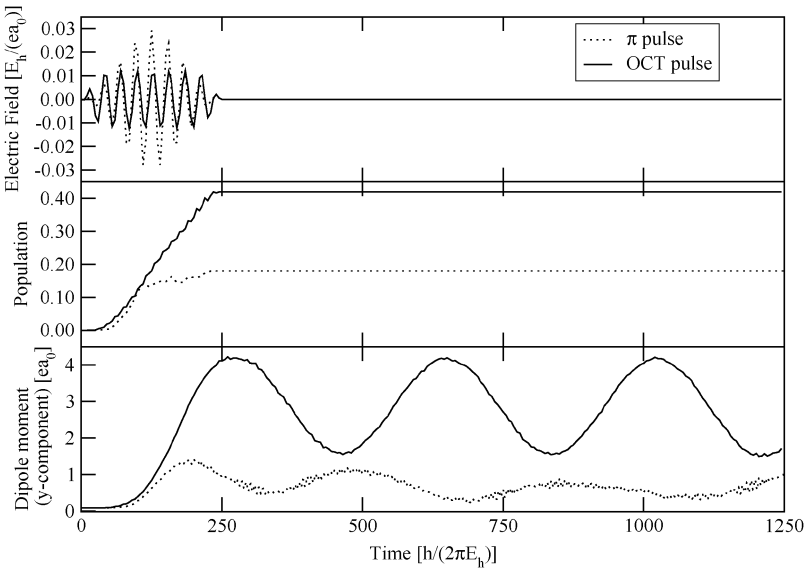

Fig. 4 Electric fields (z-component), the target state populations and the resulting dipole moments (y-component) for a short π-pulse ($\sigma = 125$, dotted line), and an optimized pulse after 20 OCT iterations (solid line).

also in this case. A wavepacket is created also in the OCT case (see lower panel), albeit a quite regular one. The oscillation period corresponds to the energy difference E_{S_2}–E_{S_1} again.

Sequential excitation $S_0 \rightarrow S_1 \rightarrow S_2$. The sequential excitation was done with two overlapping or non-overlapping π-pulses, the first one z-polarized, the second one y-polarized. The carrier frequencies were adapted to the $S_0 \rightarrow S_1$ ($\omega = \omega_{10}$) and $S_1 \rightarrow S_2$ transitions ($\omega = \omega_{21}$), respectively. For all pulses $\sigma = 2000$ was taken, which corresponds to a single pulse length of 4000. Three different delay times $\Delta t_p = t_{p,2} - t_{p,1}$ were chosen: $\Delta t_p = 0$ (fully overlapping pulses), $\Delta t_p = 2000$ (partially overlapping pulses) and $\Delta t_p = 4000$ (non-overlapping pulses), respectively. The outcome of these three computer experiments is shown, for the y-component of the dipole moment, in Fig. 5. Other π-pulse parameters are given in the Figure caption.

It is observed that for non-overlapping pulses, an almost pure S_2 state (with $P(S_2;t_f) = 0.999$ and $t_f = 8000$) is created. From the evolution of the dipole moment one observes that the first pulse quantitatively transfers population into S_1, with a dipole moment of 1.037 according to Table 1. The second pulse transfers population to S_2 as expected. The small dipole oscillations after the end of the pulse indicate a tiny rest population in S_1: The oscillation period of around 370 atomic time units fits to ω_{10} again.

When the two pulses partially overlap, a very similar final situation (with $P(S_2;t_f) = 0.998$ and $t_f = 6000$) is obtained, however, with a more gradual transition from S_0 to S_2. Finally, for fully overlapping pulses a wavepacket with comparable populations in both S_1 and S_2 is created. The large dipole oscillations reflect the large coefficients $C_i(t_f)$ ($i = 1, 2$; $t_f = 4000$), as well as the large transition dipole moment $\mu_{21,y}$ according to Table 1.

The sequential excitation can thus be as efficient as the direct excitation, provided Δt_p is not too small. Its advantage lies in the fact that lower intensities (fluences) are required. For the direct excitation, the total fluence for a π-pulse of $\cos^2$ shape

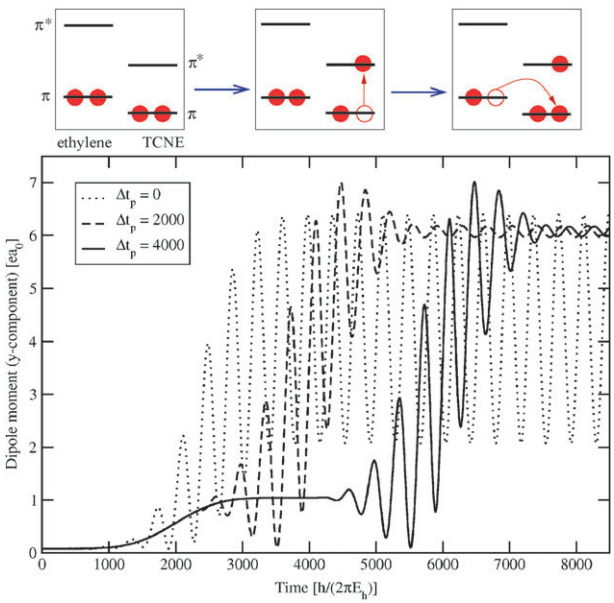

Fig. 5 Upper panel: schematic representation of the "sequential" scheme. Lower panel: dipole moment (y-component) for three π-pulse sequences. Dotted, two fully overlapping π-pulses ($\Delta t_p = 0$); dashed, partially overlapping π-pulses ($\Delta t_p = 1000$); solid, non-overlapping π-pulses ($\Delta t_p = 2000$), see text. The time step of the propagation is $\Delta t = 0.10$. The parameters for pulse 1 are: z-polarized, $\sigma = 2000$, $t_p = 2000$, $f_{0,z} = 0.0009$, $\omega = 0.2040$. The parameters for pulse 2 are: $\sigma = 2000$, $t_p = 2000 + \Delta t_p$, $f_{0,y} = 0.0007$, $\omega = 0.0167$.

and total length $t_f = 2\sigma$ is $F_{dir} = \frac{a}{t_f}\frac{1}{\mu_{02,z}^2}$, while for the sequential scheme, using two non-overlapping pulses each one also of length t_f, we have $F_{seq} = \frac{a}{t_f}\left[\frac{1}{\mu_{01,z}^2} + \frac{1}{\mu_{12,y}^2}\right]$, where $a = 3\pi c/16$ is a constant. Using the numbers of Table 1, we thus have a ratio $F_{dir}/F_{seq} \approx 2.83$.

Further investigations. Further investigations have been carried out to study laser-induced CT processes in ethylene–TCNE.

First, in view of a possible use of a CT complex as a reversible molecular switch, the question arises as to whether the state-selective D → A CT can be reversed with laser pulses. For this purpose, the selective, $S_0 \rightarrow S_2$ transition (at $R = R_0$) induced by the "long" π-pulse with $\sigma = 2000$ as shown in Fig. 3, was followed by an identical, non-overlapping second π-pulse. This second π-pulse can in principle excite the system into any of the many higher-lying states. Instead it is found to induce, almost completely, the stimulated emission from S_2 to S_0, thus completing an "on–off" switching sequence (not shown).

Secondly, it was tried to induce a charge transfer at a large distance, $R = 10.4\ a_0$ where state S_6 is the charge-transfer state as discussed earlier. Due to the larger D–A distance, the transition dipole moment is very small for direct excitation: $\mu_{60,z} = 0.0135$. As a consequence, a π-pulse would require unrealistically large intensities and thus be highly unselective. Using optimal control theory and a total pulse length of $t_f = 250$, we were able to transfer only about 0.0005 into the target state. In fact OCT gives here a pulse which is similar in shape and performance to an ordinary π-pulse. Most of the population remains in the ground state, if the D–A distance is too large (also not shown).

3.2 Larger systems: DDA, DDDA, and DAA

3.2.1 Stationary quantum chemistry. Charge transfer over very long distances is better achieved *via* molecular bridges. For that purpose, we extend our model system by stacking more donor or acceptor molecules on top of each other, along the *y*-direction. The internal geometry of the donor molecules (bond lengths, bond angles, and dihedral angles of ethylene) was fixed to those values as obtained above for the fully optimized DA system. Similarly, the internal geometry of the acceptor molecule was not reoptimized in the larger complexes. The distance between two donor or two acceptor molecules was fixed at the equilibrium donor–acceptor distance R_0. A full optimization of the structure of DDA, DDDA, DAA was not attempted because we want to focus on the possibility of simulating long-range charge transfer processes in stacked systems, rather than providing a realistic model for specific molecules.

In case of high-symmetry species such as ADA, which were not considered here, the excitation to the charge transfer state will be delocalized over both end groups. In this case, the interpretation as a directed charge transfer is not straightforward.

Then, the energies, dipole moments and transition dipole moments for all CIS states were calculated with CIS/6-31G* for a system with two donor molecules and one acceptor (DDA, see Table 3), a system with three donors and one acceptor (DDDA, see Table 4), and a system with one donor and two acceptors (DAA, see Table 5). For DDA, the 14 lowest of 226 MOs were "frozen", resulting in 6053 singlet CIS states. For DDDA, 16 out of 264 MOs were frozen, giving 8321 singlet CIS states. For DAA, 22 MOs were frozen from 338, giving 13301 singlet CIS states in total.

From the Tables one can see that the target state, which can be identified as the state with a high dipole moment which is close to the value for the transfer of a whole electron over the maximal distance, depends on system size. For DDA it is the ninth excited state S_9, with a dipole moment $\mu_{99,y}$ of about 14 ea_0, corresponding to roughly to $2eR_0$, *i.e.* an electron hopping from the outer donor to the acceptor. For DDDA, the corresponding CT state is S_{14}, with a dipole moment of over 20 ea_0 which is roughly $3eR_0$. Finally, for DAA the CT target state is S_{18}. The S_0 state is characterized by Mulliken charges Q for every monomer, which are close to zero. In the charge transfer state S_{18} the charge is somewhat delocalized: $Q_{A_1} = -0.96\ e$ (outer acceptor), $Q_{A_2} = +0.35\ e$ (inner acceptor), and $Q_D = +0.61$ e. This is why the dipole moment of S_{18} of about 11.3 ea_0, is a bit smaller than naively expected.

From the Tables it is also seen that direct excitations from S_0 to the respective target states are difficult due to prohibitively small transition dipole moments. Therefore, sequential schemes have to be used with intermediate states that are more easily accessible. For DDA, it turns out that a single intermediate state S_2 is sufficient, for DDDA, two intermediates S_2 and S_7 are useful, and finally for DAA, three intermediate states S_1, S_2, and S_3 are the most promising.

Table 3 The energies E_n, the excitation energies E_n^{exc} and the dipole moments along *y*, $\mu_{nn,y}$ for the states S_n for the system DDA. Also listed are transition dipole moments for transitions from the ground state along *z*, $\mu_{n0,z}$, and for transitions from the second excited state along *y*, $\mu_{n2,y}$. All values were calculated with CIS/6-31G*, and are given in atomic units

S_n	E_n	E_n^{exc}	$\mu_{nn,y}$	$\mu_{n0,z}$	$\mu_{n2,y}$
0	−600.9832	0.0000	0.1080	—	0.0023
2	−600.7688	0.2144	5.1382	1.2199	—
9	−600.7178	0.2654	13.9782	−0.0847	1.6240

Table 4 The energies E_n, the excitation energies E_n^{exc} and the dipole moments along *y*, $\mu_{nn,y}$ for the states S_n for the system DDDA. Also listed are transition dipole moments for transitions from the ground state along *z*, $\mu_{n0,z}$ and for transitions from the second and seventh excited states along *y*, $\mu_{n2,y}$ and $\mu_{n7,y}$. All values were calculated with CIS/6-31G*, and are given in atomic units

S_n	E_n	E_n^{exc}	$\mu_{nn,y}$	$\mu_{n0,z}$	$\mu_{n2,y}$	$\mu_{n7,y}$
0	−679.0131	0.0000	0.1220	—	−0.0021	−0.0006
2	−678.9995	0.2136	4.9857	−1.2835	—	−1.9688
7	−678.7583	0.2548	15.1885	−0.0982	−1.9688	—
14	−678.7262	0.2869	20.3210	−0.0214	−0.1054	−2.9459

Table 5 The energies E_n, the excitation energies E_n^{exc} and the dipole moments along *y*, $\mu_{nn,y}$ for the states S_n for the system DAA. Also listed are transition dipole moments for transitions from the ground state along *z*, $\mu_{n0,z}$ and for transitions from the first, second and third excited state along *y*, $\mu_{n1,y}$, $\mu_{n2,y}$, $\mu_{n3,y}$. All values were calculated with CIS/6-31G*, and are given in atomic units

S_n	E_n	E_n^{exc}	$\mu_{nn,y}$	$\mu_{n0,z}$	$\mu_{n1,y}$	$\mu_{n2,y}$	$\mu_{n3,y}$
0	−967.8609	0.0000	0.0701	—	−0.0022	0.0048	−0.0003
1	−967.6648	0.1961	0.8851	0.4498	—	−1.8181	1.2638
2	−967.6515	0.2094	4.2491	−1.3226	−1.8181	—	3.0294
3	−967.6451	0.2158	2.2435	2.3149	1.2638	3.0294	—
18	−967.5894	0.2715	11.3204	0.0371	0.9151	−0.3404	−0.4578

The transitions between the individual states are all either *z*- or *y*-polarized. Transition dipole moments between states given in the Tables which are not shown, are either exactly or close to zero. Again, the "selection rules" can be explained easily with the symmetry of the dominating orbitals involved in the transitions, in the C_{2v} point group. For instance, the $S_2 \rightarrow S_9$ transition in DDA is dominated by a π(D–D) $\rightarrow$ π^*(A) excitation, where π(D–-D) stands for an MO which is a linear combination of $\pi(D_1)$ and $\pi(D_2)$, given roughly (and without normalization) as $\pi(D–D) \sim \pi(D_1) + \pi(D_2)$. Here, D_1 denotes the outer, and D_2 the inner donor. Thus, π(D–D) transforms as A_1 under C_{2v}, while π^*(A) transforms as B_1. To get a direct product which is totally symmetric, the transition must be *y*-polarized, since $y \propto B_1$. The corresponding transition dipole moment $\mu_{92,y}$ is not only different from zero, it is also quite large because the orbital from which the electron is excited, π(D–D), has a large coefficient at the inner donor, D_2. This is why, using intermediate, delocalized states, long-range charge transfer is possible in chain-like arrangements as those studied here: in effect, the CT proceeds "stepwise", as can be seen from the gradually increasing dipole moments of intermediate states.

3.2.2 Laser-induced charge transfer dynamics

The DDA system. To demonstrate this, for the DDA system the sequential excitation to the ninth excited state *via* the second excited state is considered. For this purpose, a *z*-polarized π-pulse is used to induce a $S_0 \rightarrow S_2$ transition (corresponding to a $\pi \rightarrow \pi^*$ transition within A), as a "preparation" step. The second, *y*-polarized π-pulse induces the $S_2 \rightarrow S_9$ excitation, corresponding to a π(D–D) $\rightarrow$ π(A) transition just mentioned. Two different cases with consecutive, non-overlapping pulses have been used: In the first, the two pulses had $\sigma = 1000$, in the second $\sigma = 2000$ each, giving total (double-) pulse lengths of 4000 and 8000 atomic time units, respectively. All other pulse parameters are given in the caption to Fig. 6.

The resulting dipole moment, along *y*, is shown for both π-pulse sequences in Fig. 6. It is seen that the target dipole moment of about 14 is reached in both cases. Only low-amplitude oscillations are visible when the pulses are over, indicative of almost pure state-to-state transitions.

The DDDA system. For the DDDA arrangement, a sequential excitation to the fourteenth excited state with two pulses, *via* the second and the seventh excited state was found to be possible. Again, the first step $S_0 \rightarrow S_2$ corresponds to a "preparation" step in which an electron is excited within the acceptor ($\pi(A) \rightarrow \pi^*(A)$). This is followed by the transition from a delocalized molecular orbital $\pi(D–D–D) \approx \pi(D_1) + \pi(D_2) + \pi(D_3)$, to the acceptor orbital π(A). The third and final pulse induces a transition $S_7 \rightarrow S_{14}$, corresponding to rearrangement of charge within the D–D–D moiety and thus completing the full charge transfer.

Again, two different pulse sequences were adopted: Three non-overlapping pulses either with $\sigma = 1000$ each, or with $\sigma = 2000$ each. The pulses are *z*-, *y*-, and *y*-polarized, in this order. Other pulse parameters are given in the caption of Fig. 7, where the time-evolution of the dipole moment along *y* is shown. As can be seen from Fig. 7, in both cases the stepwise charge transfer is successful. For the longer pulses, the final dipole moment μ_y is about 20 and thus very close to the target value, $\mu_{14,14,y} = 20.3$ according to Table 4. Dipole oscillations after the pulses are off, appear to be small.

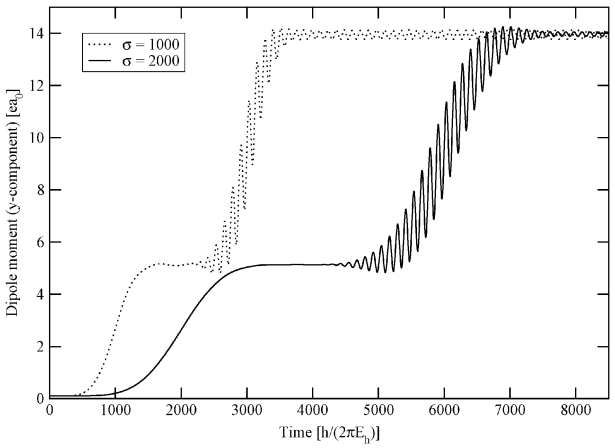

Fig. 6 Dipole moment (*y*-component) resulting from a π-pulse sequence with short pulses (dotted line) and with longer pulses (solid line), when applied to the system DDA. The time step of the propagation is $\Delta t = 0.10$. The pulse parameters are, for the dashed line: $\sigma_1 = t_{p,1} = \sigma = 1000$, $\omega_1 = 0.2144$, $f_{0,z,1} = 0.0026$; $\sigma_2 = 1000$, $t_{p,2} = 3000$, $\omega_2 = 0.0510$, $f_{0,y,2} = 0.0019$. For the solid line: $\sigma_1 = t_{p,1} = \sigma = 2000$, $\omega_1 = 0.2144$, $f_{0,z,1} = 0.0013$; $\sigma_2 = 2000$, $t_{p,2} = 6000$, $\omega_2 = 0.0510$, $f_{0,y,2} = 0.0010$.

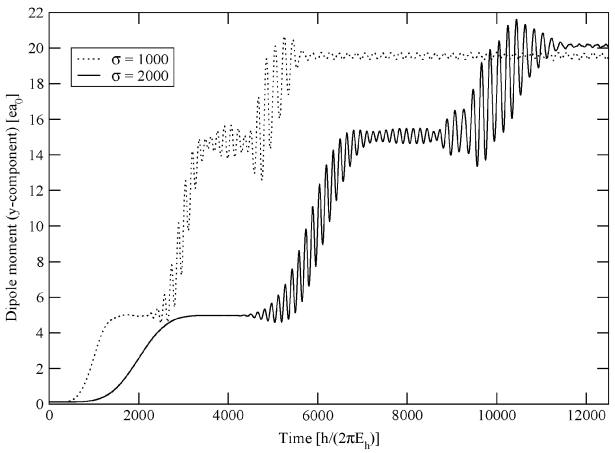

Fig. 7 Dipole moment (*y*-component) resulting from a π-pulse sequence with short pulses (dotted line) and with longer pulses (solid line), when applied to the system DDDA. The time step of the propagation is $\Delta t = 0.10$. The pulse parameters are, for the dashed line: $\sigma_1 = t_{p,1} = \sigma = 1000$, $\omega_1 = 0.2136$, $f_{0,z,1} = 0.0024$; $t_{p,2} = 3000$, $\sigma_2 = 1000$, $\omega_2 = 0.0412$, $f_{0,y,2} = 0.0016$; $t_{p,3} = 5000$, $\sigma_3 = 1000$, $\omega_3 = 0.0321$, $f_{0,y,3} = 0.0010$. For the solid line: $\sigma_1 = t_{p,1} = \sigma = 2000$, $\omega_1 = 0.2136$, $f_{0,z,1} = 0.0012$; $t_{p,2} = 6000$, $\sigma = 2000$, $\omega_2 = 0.0412$, $f_{0,y,2} = 0.0008$; $t_{p,3} = 10\,000$, $\sigma = 2000$ $\omega_3 = 0.0321$, $f_{0,y,3} = 0.0005$.

The DAA system. For DAA, the excitation of target state S_{18} with π-pulse sequences was attempted in several ways.

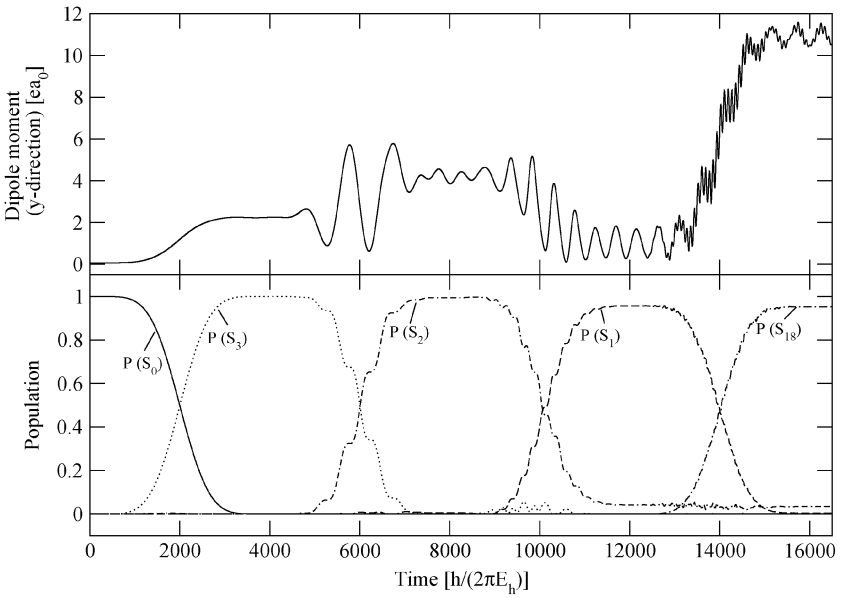

Fig. 8 CT in DAA induced by a four-pulse sequence. Shown are the resulting dipole moments (y-component) in the upper panel and the populations of five involved electronic states in the lower panel: ground state (solid line), the first (dashed line), second (dash–dash–dot), third (dotted line), and eighteenth excited state (dash–dot). The time step of the propagation is $\Delta t = 0.10$. Pulse parameters, first pulse, z-polarized: $\sigma = t_p = 2000$, $f_{0,z} = 0.0007$, $\omega = 0.2158$; second pulse, y-polarized: $\sigma = 2000$, $t_p = 6000$, $f_{0,y} = 0.0005$, $\omega = 0.0064$; third pulse, y-polarized: $\sigma = 2000$, $t_p = 10\,000$, $f_{0,y} = 0.0009$, $\omega = 0.0133$; fourth pulse, y-polarized: $\sigma = 2000$, $t_p = 14\,000$, $f_{0,y} = 0.0017$, $\omega = 0.0754$.

A two-pulse strategy $S_0 \rightarrow S_3 \rightarrow S_{18}$ was only moderately successful, due to the relatively small transition dipole moment of $\mu_{18,3,y} = -0.4578\ ea_0$ (see Table 5).

A more successful strategy is to use a four-pulse sequence with the excitation/deexcitation pattern $S_0 \rightarrow S_3 \rightarrow S_2 \rightarrow S_1 \rightarrow S_{18}$. By the two intermediate, stimulated emission processes state S_1 is reached (which is not so efficiently accessible through direct excitation), and from S_1 it is easy to populate S_{18} because the transition dipole moment is large: $\mu_{18,1,y} = 0.9151\ ea_0$. The four pulses are z-, y-, y- and y-polarized, in that order.

Using non-overlapping pulses with $\sigma = 2000$ each, the dipole moment as shown in Fig. 8, upper panel, and the populations of the five involved states as shown in the lower panel are obtained. Other field parameters are given in the figure caption. From the Figure it is evident that the population of the target state is high (about 0.952), and the final dipole moment is close to the ideal value of about 11.3.

Creation of electronic wavepackets. So far, the (uni-directional) charge transfer of an electron from one end of the molecular chain to the other was attempted by state-to-state transitions. Since only small oscillations occur at the end of the pulses, this implies only small deviations from ideal and complete state-to-state transitions. We also attempted and were successful in, creating wavepackets which mimic the formation of a localized "hole" within the molecule. As a consequence, holes (and electrons) start to move periodically, leading to large-amplitude oscillations in the dipole moment. This type of electron/hole dynamics is similar to that suggested recently,[39] and will be considered in greater detail elsewhere.[40]

4. Conclusions

In this paper, we applied the explicitly time-dependent TD-CIS method to treat laser-pulse-induced charge transfer in a donor–acceptor (DA) system, ethylene–TCNE. The method nicely accounts for low-lying, bound charge-transfer states, also for larger aggregates such as DDA, DDDA, and DAA. Different strategies were suggested to populate the target CT states: by direct excitation using single π-pulses, by indirect excitation using sequences of π-pulses, and, finally, pulses created from optimal control theory. For DA, all strategies work well. For the larger aggregates, on the other hand, direct excitation corresponds to a long-range charge transfer which is prohibited by small transition dipole moments. This would cause the need for high intensities, which in turn destroys state-selectivity. Indirect pathways, however, offer "mild" conditions since the excitation process makes use of delocalized orbitals and stepwise charge transfer. In the calculations, all excited singlet states were accounted for because the truncation of the state space can lead to serious errors when ultrashort, intense pulses are used.[33]

It should be noted that TD-CIS is not a method which describes general valence excitations quantitatively correct. However, it was demonstrated that the method can be systematically improved towards the "exact" answer when higher excitations are accounted for ref. 22. In cases when the Hilbert space becomes too large, a perturbative treatment of higher excitations is useful.[22] With ultrashort pulses, many ionizing (CIS) states above the ionization potential are temporarily populated. However, during the short times considered here, these states can be approximated as bound to a good approximation. In fact, preliminary calculations in

which states with $E_i^{\mathrm{CIS}} > 0$ were complemented by an imaginary potential $-\frac{\mathrm{i}}{2}\Gamma_\mathrm{i}$ to model the ionization with a rate Γ_i show that state-to-state transitions are often unaffected. Finally, the TD-CI method also offers the possibility to treat dissipation and/or spontaneous emission.[23] Other non-radiative processes, such as non-Born–Oppenheimer and spin–orbit couplings, should be easy to implement. Work along several of these lines is in progress in our laboratory.

Acknowledgements

This work was supported by Sonderforschungsbereich 450 of the Deutsche Forschungsgemeinschaft, Analysis and Control of Ultrafast Photoinduced Processes (subproject C7).

References

1 M. Dantus, M. J. Rosker and A. H. Zewail, *J. Chem. Phys.*, 1987, **87**, 2395.
2 T. S. Rose, M. J. Rosker and A. H. Zewail, *J. Chem. Phys.*, 1988, **88**, 6672.
3 M. Hentschel, R. Kienberger, Ch. Spielmann, G. A. Reider, N. Milosevic, T. Brabec, P. Corkum, U. Heinzmann, M. Drescher and F. Krausz, *Nature*, 2001, **414**, 509.
4 M. Drescher, M. Hentschel, R. Kienberger, M. Uiberacker, V. Yakovlev, A. Scrinzi, Th. Westerwalbesloh, U. Kleineberg, U. Heinzmann and F. Krausz, *Nature*, 2002, **419**, 803.
5 E. Runge and E. K. U. Gross, *Phys. Rev. Lett.*, 1984, **52**, 997.
6 M. E. Casida, C. Jamorski, K. C. Casida and D. R. Salahub, *J. Chem. Phys.*, 1998, **108**, 4439.
7 A. Dreuw, J. L. Weisman and M. Head-Gordon, *J. Chem. Phys.*, 2003, **119**, 2943.
8 D. J. Lacks and R. G. Gordon, *Phys. Rev. A*, 1992, **47**, 4681.
9 M. E. Casida, F. Gutierrez, J. Guan, F.-X. Gadea, D. Salahub and J.-P. Daudey, *J. Chem. Phys.*, 2000, **113**, 7062.
10 D. J. Tozer, *J. Chem. Phys.*, 2003, **119**, 12697.
11 O. Gritsenko and E. J. Baerends, *J. Chem. Phys.*, 2004, **121**, 655.
12 N. T. Maitra, *J. Chem. Phys.*, 2005, **122**, 233104.
13 W. Hieringer and A. Görling, *Chem. Phys. Lett.*, 2006, **419**, 557.
14 A. D. Becke, *J. Chem. Phys.*, 1993, **98**, 5648.
15 T. Klamroth, *Phys. Rev. B*, 2003, **68**, 245421.
16 C. Huber and T. Klamroth, *Appl. Phys. A*, 2004, **81**, 91.
17 P. Saalfrank, T. Klamroth, C. Huber and P. Krause, *Isr. J. Chem.*, 2005, **45**, 205.
18 H. B. Schlegel, S. Smith and X. Li, *J. Chem. Phys.*, 2007, **126**, 244110.
19 P. Krause, T. Klamroth and P. Saalfrank, *J. Chem. Phys.*, 2005, **123**, 074105.
20 P. Krause and T. Klamroth, *J. Chem. Phys.*, 2008, **128**, 234307.
21 P. Krause, *Many-electron Dynamics in Molecules by means of Time-dependent Configuration Interaction Methods*, PhD dissertation, University of Potsdam, 2007.
22 P. Krause, T. Klamroth and P. Saalfrank, *J. Chem. Phys.*, 2007, **127**, 034107.
23 J. C. Tremblay, T. Klamroth and P. Saalfrank, *J. Chem. Phys.*, 2008, **129**, 084302.
24 J. Zanghellini, M. Kitzler, C. Fabian, T. Brabec and A. Scrinzi, *Laser Phys.*, 2003, **13**, 1064.
25 T. Kato and H. Kono, *Chem. Phys. Lett.*, 2004, **392**, 533.
26 M. Nest, T. Klamroth and P. Saalfrank, *J. Chem. Phys.*, 2005, **122**, 124102.
27 A. D. Bandrauk, E. Aubanel and S. Chelkowski, in *Femtosecond Chemistry*, ed. J. Manz and L. Wöste, Verlag Chemie, Weinheim, 1995, ch. 25, vol. 2, p. 731.
28 I. I. Rabi, *Phys. Rev.*, 1937, **51**, 652.
29 S. Shi, A. Woody and H. Rabitz, *J. Chem. Phys.*, 1988, **88**, 6870.
30 R. Kosloff, S. A. Rice, P. Gaspard, S. Tersigni and D. J. Tannor, *Chem. Phys.*, 1989, **139**, 201.
31 W. Zhu, J. Botina and H. Rabitz, *J. Chem. Phys.*, 1998, **108**, 1953.
32 W. Zhu and H. Rabitz, *J. Chem. Phys.*, 1998, **109**, 385.
33 T. Klamroth, *J. Chem. Phys.*, 2006, **124**, 144310.
34 P. C. Hariharan and J. A. Pople, *Theor. Chim. Acta*, 1973, **28**, 213.
35 M. J. Frisch, G. W. Trucks, H. B. Schlegel, G. E. Scuseria, M. A. Robb, J. R. Cheeseman, J. A. Montgomery, Jr., T. Vreven, K. N. Kudin, J. C. Burant, J. M. Millam, S. S. Iyengar, J. Tomasi, V. Barone, B. Mennucci, M. Cossi, G. Scalmani, N. Rega, G. A. Petersson, H. Nakatsuji, M. Hada, M. Ehara, K. Toyota, R. Fukuda, J. Hasegawa, M. Ishida, T. Nakajima, Y. Honda, O. Kitao, H. Nakai, M. Klene, X. Li, J. E. Knox, H. P. Hratchian, J. B. Cross, V. Bakken, C. Adamo, J. Jaramillo, R. Gomperts, R. E. Stratmann, O. Yazyev, A. J. Austin, R. Cammi, C. Pomelli, J. Ochterski, P. Y. Ayala, K. Morokuma, G. A. Voth, P. Salvador, J. J. Dannenberg, V. G. Zakrzewski, S. Dapprich, A. D. Daniels, M. C. Strain, O. Farkas, D. K. Malick, A. D. Rabuck, K. Raghavachari, J. B. Foresman, J. V. Ortiz, Q. Cui, A. G. Baboul, S. Clifford, J. Cioslowski, B. B. Stefanov, G. Liu, A. Liashenko, P. Piskorz, I. Komaromi, R. L. Martin, D. J. Fox, T. Keith, M. A. Al-Laham, C. Y. Peng, A. Nanayakkara, M. Challacombe, P. M. W. Gill, B. G. Johnson, W. Chen, M. W. Wong, C. Gonzalez and J. A. Pople, *GAUSSIAN 03 (Revision C.02)*, Gaussian, Inc., Wallingford, CT, 2004.
36 A. D. Becke, *J. Chem. Phys.*, 1986, **84**, 4524.
37 J. P. Perdew and W. Yue, *Phys. Rev. B*, 1986, **33**, 8800.
38 M. W. Schmidt, K. K. Baldridge, J. A. Boatz, S. T. Elbert, M. S. Gordon, J. J. Jensen, S. Koseki, N. Matsunaga, K. A. Nguyen, S. J. Su, T. L. Windus, M. Dupuis and J. A. Montgomery, *J. Comput. Chem.*, 1993, **13**, 1347.
39 S. Lünnemann, A. I. Kuleff and L. S. Cederbaum, *J. Chem. Phys.*, 2008, **129**, 104305.
40 S. Klinkusch, T. Klamroth and P. Saalfrank, to be published.

